PHYSICAL REVIEW B **95**, 094103 (2017)

Ubiquity of quantum zero-point fluctuations in dislocation glide

Marie Landeiro Dos Reis, Anshuman Choudhury, and Laurent Proville
DEN-Service de Recherches de Métallurgie Physique, CEA, Université Paris-Saclay, F-91191 Gif-sur-Yvette, France
(Received 9 December 2016; published 8 March 2017)

Modeling the dislocation glide through atomic scale simulations in Al, Cu, and Ni and in solid solution alloys Al(Mg) and Cu(Ag), we show that in the course of the plastic deformation the variation of the crystal zero-point energy (ZPE) and the dislocation potential energy barriers are of opposite sign. The multiplicity of situations where we have observed the same trend allows us to conclude that quantum fluctuations, giving rise to the crystal ZPE, make easier the dislocation glide in most materials, even those constituted of atoms heavier than H and He.

DOI: 10.1103/PhysRevB.95.094103

I. INTRODUCTION

The implication of quantum mechanics in plasticity of crystals has long been a matter of theoretical investigations. The main efforts were concentrated on accounting for interactions between phonons and dislocations [1–3] because they are the key physical ingredients in the process of conversion of plastic work into heat during deformation [4,5] as well as in the process of thermal activation of dislocation glide [1,6]. Modern simulation tools [7,8] have allowed us recently to supplement the theory and shed new light on the low-temperature deformation tests. Employing atomic scale simulations based on the embedded atom method (EAM) [9,10] it was found that along the dislocation glide the zero-point energy (ZPE), which in the harmonic approximation is merely the sum of phonon frequencies times half $\hbar$, varies with an amplitude of same order as the dislocation Peierls barrier but with an opposite sign. The variation of the ZPE was found to yield a significant Peierls stress reduction for the screw dislocation in body-centered-cubic (bcc) Fe [7]. This result showed how quantum fluctuations could be involved in the plasticity of certain metals even though they are constituted of atoms with some relatively heavy masses in comparison with conventional quantum crystals [11] as solid He or H_2. A recent experimental study by Caillard [12] of the deformation of bcc Fe thin foils confirms the emergence of additional contributions to the screw dislocation thermally activated glide at low temperatures which might be ascribed to quantum fluctuations.

In the present study we question the generality of the ZPE contribution to plastic deformation in solids. In order to achieve a pertinent answer, the phonon frequencies have been computed in different face-centered-cubic (fcc) crystals, i.e., Al, Ni, and Cu and solid solutions Al(Mg) and Cu(Ag), for both dislocation types, i.e., edge and screw. In pure crystals, our work reveals that the variations of the ZPE have same order of magnitude as the Peierls barriers and they are of opposite sign. Interestingly, in the 3 crystals the dislocations are dissociated in their glide planes with different widths of the stacking fault ribbon. Their features, the geometry of their core and the height of their Peierls barriers, contrast with those for screw dislocations in bcc Fe, the core of which presents a specific compactness [13]. Therefore the fact that ZPE variations remain significant in comparison to the Peierls barriers for different core geometry can be viewed as the demonstration of their ubiquity. In order to explore further the ZPE effect in plastic deformation, our computations of phonons in the course of crystal deformations have been extended to the case of solid solutions alloys, Al(Mg) and Cu(Ag) where solute atoms hinder the dislocation glide [14,15]. According to the position of the solute atom the interaction with the dislocation may be either repulsive or attractive and therefore the sign of the potential energy barrier changes. However in both situations the ZPE variations have been found to be opposite to the potential energy barrier. We conclude that the variations of quantum ZPE may yield a softening of solid solutions at low temperatures.

The atomic scale simulations based on modeling atom interactions through EAM potentials present some uncertainties with respect to dislocation properties [16]. Thus it is of primary importance to verify a prediction by means of multiple examinations in different systems. It is exactly the purpose of the present work which allows us to prove the implication of quantum fluctuations in plastic deformation at low temperatures in various model materials, pure metals as well as binary alloys.

The present paper is organized as follows. First, in Sec. II the simulation cell construction and the simulation method for the dislocation glide are described together with the computation of the crystal ZPE. The results are analyzed in Sec. III, while our conclusions are presented in Sec. IV.

II. ATOMIC SCALE CALCULATIONS

To model the interaction between the atoms in fcc crystals we have considered various interaction potentials based on the embedded atom method (EAM). Some are for pure crystals such as Al [10], Cu [17], and Ni [18] while others are for binary alloys such as Al(Mg) [19,20] and Cu(Ag) [21].

To study the dislocations at the atomic scale, we have built a simulation cell with several thousands of atoms with fcc crystal symmetry. An example has been reported in Fig. 1. A dislocation either of screw type or of edge type is introduced as described in earlier works [22–25]. The geometry of the cell was set up with the following crystal orientations: the [110] direction along the X axis, the $[\bar{1}12]$ direction along the Y axis, and the $[1\bar{1}1]$ direction along the Z axis. The dislocation's Burgers vector is $b = \frac{a_0}{2}[110]$, which corresponds either to the glide direction for the edge dislocation or to the line direction of the screw dislocation. Here, a_0 represents the lattice parameter of the perfect fcc lattice. Two surfaces have been created, each with a normal corresponding to the Z

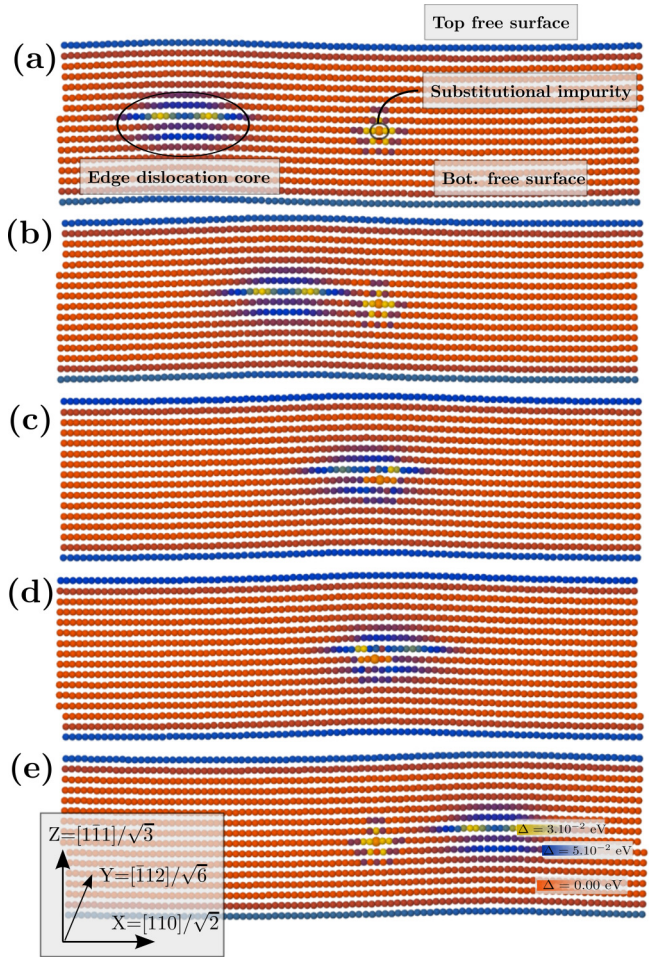

FIG. 1. (a)–(e) Snapshots of the crossing process for an $a_0/2[110](1\bar{1}1)$ edge dislocation in a fcc Al crystal with a single Mg impurity situated in substitution in the first crystal plane underneath the dislocation glide plan. The colors of atoms are fixed according to their potential energy deviations Δ_i from perfect crystal cohesive energy per atom (see text). Some examples have been reported in Fig. 1(e).

direction, above and beneath the crystal sample, forming a slab as shown in Fig. 1. A constant external shear stress σ_{xz} may be applied by apportioning constant forces over the atoms involved in the surfaces. The value of such atomic forces is merely $\pm S\sigma_{xz}/N_{surf}$ where N_{surf} is the number of atoms at the surface, whose the total area is denoted by S. The sign of the applied forces depends on which surface is considered; in the present case we have chosen $+$ for the surface on top and $-$ for the surface underneath the crystal. To introduce the dislocations, the atoms are initially displaced according to the corresponding isotropic elastic solution [26]. In order to avoid the effect of additional free surfaces and to consider yet a relatively small number of atoms, we impose periodic boundary conditions along X and Y. When a screw dislocation type is considered, an additional shift in the X direction [22] is introduced in the computation of distances between two atoms associated with a bond, which crosses the Y boundary. Strictly speaking the boundary conditions are no longer periodic but this ingenious trick was found to stabilize the simulation cell with a single screw dislocation [27]. The use of such a method allows us to reduce the number of atoms that are involved in the simulation cell in comparison to the other possibilities, where some dislocations of different sign must be introduced to fulfill the strict periodicity of the cell [22]. When one has considered an edge dislocation type, the conditions are periodic in both directions X and Y. One half crystal plane orthogonal to the X direction is removed and the size of the simulation cell along the same direction is adapted to relax the whole energy of the cell [23]. The atomic positions are relaxed by adding a simple Langevin damping into the dynamical equation of motion, which is integrated with a standard velocity Verlet algorithm [28]. After a relaxation corresponding to a maximum atomic force below 10^{-4} eV/Å the simulation cell reaches mechanical equilibrium and reducing further the force accuracy does not modify our results. As expected for fcc crystals, because of their relatively small stacking fault energies, the dislocation cores split into two partial dislocations separated by a stacking fault, the width of which is material dependent. It is clearly seen in Fig. 1(a) where the atoms have been colored according to their potential energy deviation from their energy in the perfect crystal without dislocation. If the atom is identified by the number i, we denote by E_i^0 the reference energy, which can easily be computed before introducing the dislocation in the simulation cell. Denoting by E_i the potential energy of atom i, the potential energy deviation is given by $\Delta_i = E_i - E_i^0$. In the case where no impurity is present in the crystal, E_i^0 can be substituted by the crystal cohesive energy per atom, E_{coh}.

In the EAM models [29], the atomic energy is given by the functional

$$E_i = \frac{1}{2}\sum_{j=\langle i\rangle} V(r_{ij}) + F\left(\sum_{j=\langle i\rangle}\rho(r_{ij})\right), \qquad (1)$$

where the sum's subscript runs over the neighbors j of the atom i, r_{ij} is the distance between these atoms (smaller than r_c, the cutoff radius defined in the EAM adjustment), V corresponds to a pair potential, ρ to the electronic density function, and F stands for the embedding function.

The recent progress into the accuracy of EAM is based on its adjustment with a data basis built from *ab initio* calculations [10], which may involve dislocation configurations [30]. The development of *ab initio* computations has allowed us to calculate fundamental features of dislocations such as their core geometry, their glide plane, and their Peierls barriers [16,31,32]. Such computations being very limited in size, i.e., a few hundred atoms, the study of dislocations in solids still requires the development of atomic potential interactions such as those based on EAM.

The dimension of the simulation cells along Z is $8\sqrt{3}a_0$ while the sizes in X and Y are adapted to the dislocation type. For an edge dislocation, the Burgers vector is along X and the dislocation dissociates and glides along the same direction such that this dimension must be large enough to avoid spurious interactions with the periodic images. We have found that with an X dimension of $45\sqrt{3}a_0/2$, the periodic image effect is negligible. Along Y, we have reduced the dimension to $6\sqrt{3/2}a_0$. The latter constraint is imposed by the fact that our main purpose is to compute the eigenfrequencies of the

entire simulation cell which is computationally very heavy since this operation requires the diagonalization of the Hessian matrix with $3N_{\rm at}$ rank, where $N_{\rm at}$ stands for the total number of atoms. The consequence of such a reduction along Y is that we are compelled to study straight dislocations because of the translational symmetry. Thence the dislocation bowing cannot be considered in the present work. However we have tested an approximation, presented hereafter for the computation of the Hessian eigenvalues which should allow us to extend our work to larger simulation cells where the dislocation bowing could be accounted for (see Einstein approximation further in the text). For a screw dislocation, the Burgers vector is along X and the dislocation dissociates and glides along the Y direction such that we have found that a dimension of $50\sqrt{3/2}a_0$ in the Y direction is required to avoid periodic image effects. Then along X, we have reduced the dimension to $6\sqrt{3}a_0/2$ for the same reasons as for the edge dislocation.

By increasing gradually the applied stress and relaxing the atomic positions through the Verlet-Langevin algorithm, the dislocation starts gliding once the stress reaches a certain stress threshold corresponding to the dislocation Peierls stress. In the case where an impurity is situated close to the glide plane of the dislocation (as shown in Fig. 1), the stress threshold is larger than the Peierls stress which is representative of solid solution hardening [15]. Once the applied stress has been fixed such that the dislocation can glide freely into the simulation cell, we proceed to a periodic saving of atomic configurations which are used afterward as initial configuration in the nudged elastic band method (NEB) [33]. The NEB method is run with no applied stress such that the minimum energy path (MEP) is computed with no effect of stress. We have employed between 200 and 300 NEB images in order to determine precisely the MEP which is plotted according to dislocation position in Figs. 2(a)–2(d) for different systems. The position of the dislocation is determined as the barycenter of the atomic positions weighted by Δ_i. Thence for an edge dislocation the position along the X axis is simply written

$$X_D = \frac{1}{\sum_i \Delta_i} \sum_i x_i \Delta_i, \tag{2}$$

while the position along the Z axis is given by

$$Z_D = \frac{1}{\sum_i \Delta_i} \sum_i z_i \Delta_i, \tag{3}$$

where x_i and z_i are the coordinates of atom i along the X and Z axis, respectively. For the screw dislocation the position along the Y axis is given by

$$Y_D = \frac{1}{\sum_i \Delta_i} \sum_i y_i \Delta_i, \tag{4}$$

while its position along the Z axis is also given by Eq. (3). The dislocation position can be obtained from other considerations detailed in the literature (see for instance [34,35] and references therein). The main interests of the definition employed here are (i) its simplicity to be implemented with EAM and (ii) it can be generalized to other crystal defects such as vacancies and interstitial atoms. Then, the three equations (2), (3), and (4) would be involved to fully determine the defect position in the three dimensions of space. We have also verified the ability of the present definition to determine the positions of different dislocation segments in the cases of longer dislocations with wavy profiles and even with kinked profiles such as the ones encountered in bcc crystals.

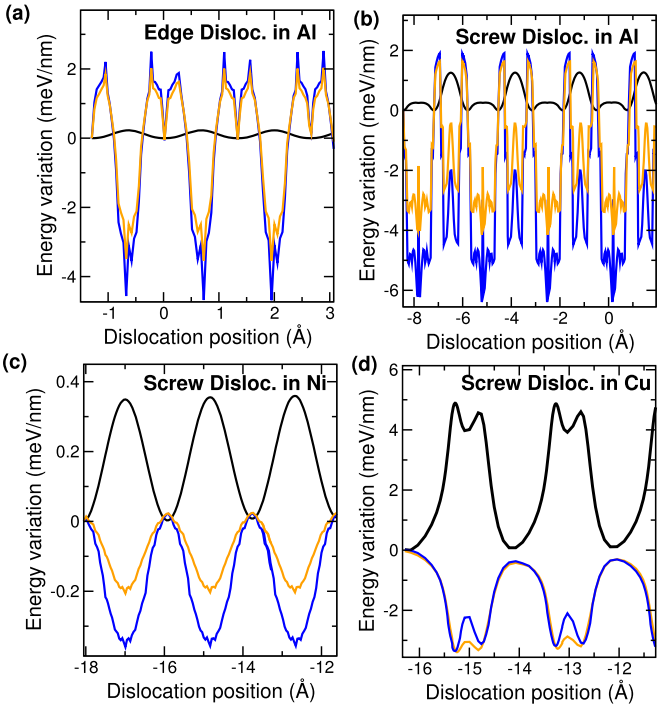

FIG. 2. (a)–(d) Peierls barriers (black lines) computed from the NEB method for different dislocations in various fcc crystals and the corresponding zero-point energy variations computed from the exact diagonalization of the full crystal Hessian (blue) and from the Einstein approximation detailed in the text (orange). The atomic scale model for Al is from [10,19] while those for Ni and Cu are from [18] and [17], respectively.

The computations of the Hessian matrix coefficients have been performed through the calculation of the first derivative of forces under the finite displacements of each atom in the three directions of space. When the atom denoted by i is displaced in direction d_i, the whole force field must be computed over each neighbor j, in each direction labeled by d_j. Denoting by $F_{d_j,j}$ the force exerted on atom j in the direction d_j and by $X_{d_i,i}$ the displacement of atom i in the direction d_i, the coefficient of the Hessian matrix situated at row $i + N_{\rm at}(d_i - 1)$ and column $j + N_{\rm at}(d_j - 1)$ is given by

$$\mathcal{H}_{i+N_{\rm at}(d_i-1),\, j+N_{\rm at}(d_j-1)} = -\frac{1}{\sqrt{m_i m_j}} \frac{\delta F_{d_j,j}}{\delta X_{d_i,i}}, \tag{5}$$

where m_i and m_j correspond to the masses of atom i and j, respectively. A good computation of the discrete force derivative in Eq. (5) is obtained when averaged over several atomic displacements of one hundredth of an angstrom. This procedure has been tested in comparison to the exact computation which is possible when considering analytical potentials. The diagonalization of the matrix $\mathcal{H}$ has been performed with the routine named DSPEV from the linear algebra package LAPACK [36]. The $3N_{\rm at}$ eigenvalues of $\mathcal{H}$ are denoted by λ_u where the subscript u runs from 1 to $3N_{\rm at}$. The

zero-point energy of the system is then evaluated through the harmonic approximation by

$$Z = \frac{\hbar}{2} \sum_{u=1}^{3N_{\text{at}}} \sqrt{\lambda_u}. \tag{6}$$

The zero-point energy is computed all along the MEP from the Hessian diagonalization of each NEB image. We have ascribed the label n to the nth NEB image such that the corresponding zero-point energy is denoted by Z_n. Along the MEP, the system passes from stable configurations to unstable ones such that in the Hessian spectrum one eigenvalue becomes negative indicating the emergence of an unstable mode for which $\lambda_u < 0$. The contribution of such a mode is excluded from the zero-point energy evaluation in Eq. (6) since the amplitudes of the associated imaginary frequencies given by $\sqrt{|\lambda_u|}$ remain negligible in comparison to the variations of the zero-point energy along the MEP, given by $\delta Z_n = Z_n - Z_0$. The latter has been reported in Figs. 2(a)–2(d) against the dislocation position in different fcc crystals.

III. THEORETICAL ANALYSIS OF ATOMIC SIMULATIONS

In Figs. 2(a)–2(d), we have reported our results for the Peierls barriers and the associated ZPE variation of different dislocations in different fcc crystals. According to the EAM potentials that we have selected to model fcc crystals, the amplitude of the Peierls barriers varies between a tenth of an meV/nm to 5 meV/nm. The shape of the barrier is similar to a sinusoidal such as for edge dislocation in Al [Fig. 2(a)] or for screw dislocation in Ni [Fig. 2(c)]. But it may also be composed of the superimposition of different periodic functions, such as for screw dislocation in Al and Cu [Figs. 2(b) and 2(d)]. This shape depends on the manner of the Shockley partial dislocation [26] glide, i.e., the profile of their energy barriers and the strength of their bounds.

For comparison we have also reported in Figs. 2(a)–2(d) the ZPE variations δZ_n against the dislocation position. For the screw type dislocation in Cu the maximum variation of the ZPE is of the order of one half the Peierls barrier height, i.e., similar to what was found for screw dislocations in α-Fe [8]. More interestingly the ZPE variation is negative around the Peierls barrier maximum which means that quantum fluctuations are less important at the top of the barrier and hence the barrier crossing is easier because of such quantum fluctuations reduction along the MEP [7]. The negative ZPE variation has an amplitude which is comparable to the Peierls barrier for the screw dislocation in Ni Fig. 2(c), while in Al, for both types of dislocation Figs. 2(a) and 2(b) the amplitude of ZPE variation is even larger than the Peierls barriers. Here we must emphasize that (i) our computation relying upon the quantization of the harmonic modes provides a rough estimation of quantum effects which neglects anharmonic contributions and (ii) the atomic interaction EAM models may yield large uncertainties. Nevertheless the same trend is observed in the four different cases presented in Figs. 2(a)–2(d) which we consider as a confirmation that quantum fluctuations cannot be ignored in the low-temperature plasticity of crystals. According to the quantum harmonic theory employed here, one can expect that

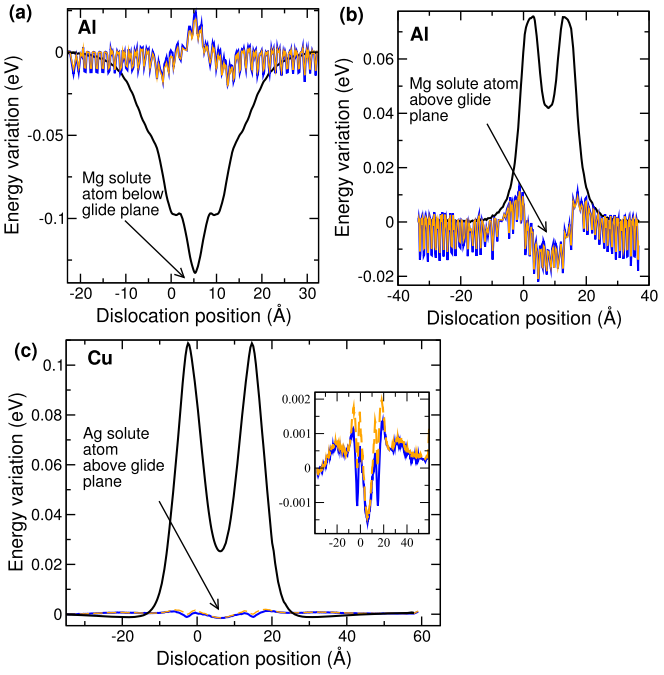

FIG. 3. Energy barriers (black) computed from NEB method for an edge dislocation crossing an impurity situated in substitution in different fcc crystals and the corresponding zero-point energy variations computed from the exact diagonalization (blue) and from the Einstein approximation detailed in the text (orange). Atomic scale model for Al(Mg) [(a), (b)] is taken from [19] while the model for Cu(Ag) (c) is from Ref. [21]. In (a) the position of the solute atom is below the glide plane while in (b) and (c) the solute atom is situated above the glide plane. The inset in (c) shows the ZPE variation associated with dislocation glide in Cu(Ag).

the crystal quantum fluctuations are large enough to reduce the effect of the Peierls barriers the dislocations have to overpass. In the absence of thermal effects, this fact can be understood from the mere consideration that the whole energy of the system is composed of the sum of (i) the potential energy which is computed from the EAM interaction potential and (ii) the zero-point energy which is itself the result of a combination between kinetic and vibrational energies. Since our results show that the ZPE variation is negative when the Peierls barrier is maximum, it implies that the total energy barrier to overpass is lower than what could be expected from the sole consideration of potential energy.

In order to examine the effect of quantum fluctuations on the dislocation depinning from solute atoms, we have repeated our computations for a simulation cell where a solute atom has been placed in the vicinity of the dislocation glide plane. The results are reported in Figs. 3(a) and 3(b) for an edge dislocation in a crystal of Al with one Mg atom introduced in the simulation cell in substitution to one Al atom situated either below [Fig. 3(a)] or above [Fig. 3(b)] the dislocation glide plane. For simplicity we have considered only the situations where the Mg atoms are in the two $(1\bar{1}1)$ planes that adjoin the glide plane. In order to cover the whole range of interaction between the dislocation and the solute atoms, the NEB method has been performed with starting and ending states where the dislocation is situated far from

the solute atom. The variations of the interaction energy that are found here agree with previous publications [15,37]. When the Mg atom is below the glide plane [Fig. 3(a)] the interaction is attractive whereas when the Mg atom is above the glide plane, the interaction is repulsive [Fig. 3(b)]. In both case, the large oscillations of the ZPE due to the crossing of the crystal Peierls barriers are superimposed on the ZPE variation related to the dislocation interaction with the Mg atom. However the former corresponds to a wavelength of the order of interatomic distances in the crystal while the variation of the latter extends over 20 to 40 Å. One can therefore distinguish well the variations associated with the Peierls barrier crossing from the one due to the dislocation interaction with the solute atom. In the situation where the Mg atom is below the glide plane the ZPE varies as the inverse of the interaction potential. In Fig. 3(a), the ZPE variation is positive when the interaction potential is minimum which means that the quantum effects ease the depinning of the dislocation from the Mg solute atom. In Fig. 3(b), we distinguish two maxima in the interaction potential which correspond to the crossing between the Shockley partial dislocations and the Mg atom. The system is metastable when the Mg atom is situated at the middle of the stacking fault ribbon associated with the dislocation core split into partial dislocations. When the partial dislocations cross the Mg atom the ZPE increases and it follows the trend of the interaction potential. We distinguish clearly in Fig. 3(b) that the ZPE reaches some local maxima at positions where the interaction potential is not maximal. Actually the ZPE maxima, culminating roughly at one tenth of the interaction potential maximum, are situated in a region where the potential interaction is around one third of its maximum. On the contrary when the potential interaction is maximal the ZPE is close to naught. We conclude that the ZPE variation does not contribute to increasing the energy barrier of the Shockley partial dislocations. However when the Mg atom passes into the stacking fault ribbon the ZPE decreases and it reaches a value smaller than the ZPE when the dislocation is far from the Mg atom. This means that the ZPE contributes to stabilizing the presence of Mg atoms into the stacking fault ribbon and that the repulsive interaction between the Mg atoms and the dislocation is mitigated by ZPE. In both situations, for Mg atoms situated below [Fig. 3(a)] or above [Fig. 3(b)] the glide plane, corresponding to attractive and repulsive interactions, respectively, the ZPE tends to ease the dislocation glide.

Similar computations have been performed in the system Cu(Ag) with the EAM model from [21] but the magnitude of quantum effects is smaller. In Fig. 3(c), we have reported the computation results for an edge dislocation crossing an impurity atom situated above the glide plane. The potential barrier is higher than for Al(Mg) while the ZPE variation is one order of magnitude smaller [see the inset in Fig. 3(c)]. In the case of Cu(Ag) one can conclude that the ZPE contribution is negligible according to the EAM model employed here.

To gain some insight into the ZPE variation along the MEP of dislocations, we have tested the approximation which consists of computing eigenfrequencies from the on-site frequencies of each atom considering the other atoms as frozen. Then we consider the solid as an assembly of independent single oscillators, which corresponds to the Einstein approximation. The main interest of such approximation is that the numerical diagonalization of the Hessian is skipped. By combination of Eq. (5) and Eq. (6), the Einstein approximation for ZPE of the whole simulation cell is

$$Z_{\mathrm{E}} = \frac{\hbar}{2} \sum_{i,d_i} \sqrt{-\frac{\delta F_{d_i,i}}{m \delta X_{d_i,i}}}. \tag{7}$$

The variation of ZPE computed with Eq. (7) has been reported in Figs. 2(a)–2(d) and in Figs. 3(a)–3(c). In all cases, we notice a good agreement between the Einstein approximation in Eq. (7) and the exact computation of the eigenfrequencies obtained by diagonalization of the Hessian matrix. We have verified (see Fig. 4) that the same agreement is also obtained in the case of straight screw dislocation gliding in different

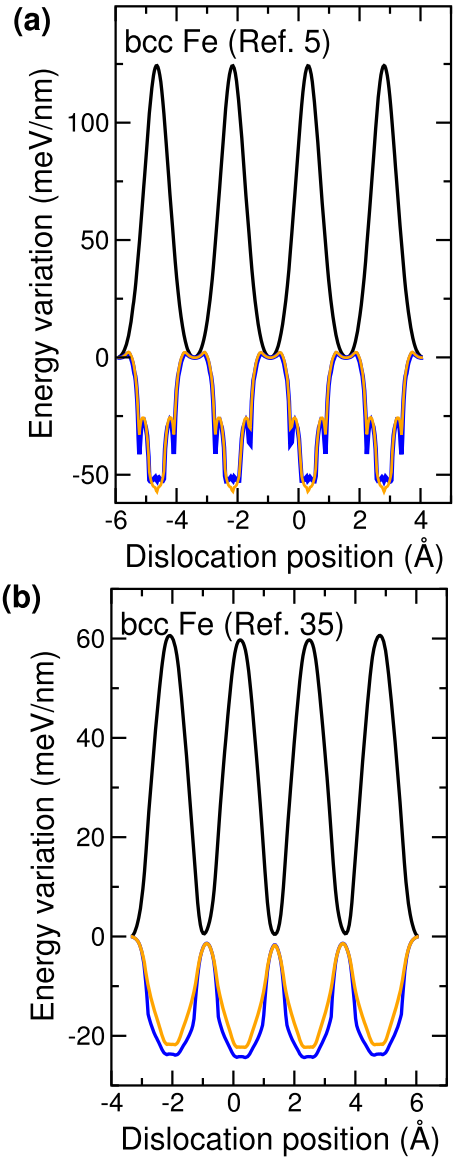

FIG. 4. (a), (b) Energy barriers (black) computed from NEB method for a straight screw dislocation in α-Fe and the corresponding zero-point energy variations computed from the exact diagonalization (blue) and from Einstein approximation detailed in the text (orange). Atomic scale model for α-Fe is from Refs. [7] and [38].

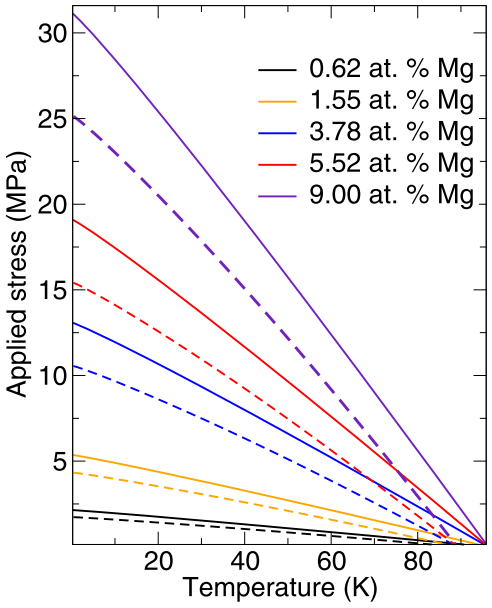

FIG. 5. Stress-temperature curve obtained from the computation detailed in the Appendix for solid solutions Al(Mg) with different concentrations. The full lines represent the result from a classical calculation Eq. (A10) and the dashed lines are obtained from Eq. (A7) accounting for quantum statistics of the crystal vibrational modes. The solid solution concentrations are those studied in Ref. [39].

bcc iron models [7,38]. The good agreement between the Einstein approximation and the exact ZPE calculation through the diagonalization of the Hessian matrix shows that the main quantum contribution comes from vibrational modes with short wavelengths since the acoustic modes are skipped through the Einstein approximation.

In order to evaluate how the critical resolved shear stress (CRSS) of a solid solution is modified by the ZPE contribution, we have applied the transition state theory as presented in Ref. [7]. The details of our derivation have been reported in the Appendix where quantum statistical mechanics and classical statistical mechanics have been used to obtain Eq. (A7) and Eq. (A10), respectively. The comparison between Eq. (A7) and Eq. (A10) allows us to work out a shift of the CRSS proportional to δZ_s, the difference between the ZPE at saddle state and the ZPE at ground state. Our estimation for the CRSS in Al(Mg) solid solution at different concentrations has been reported in Fig. 5 where one can notice clearly the softening due to a negative ZPE difference between the saddle state and the ground state.

IV. CONCLUSION

We have reported our study of the variation of quantum zero-point energy (ZPE) along the minimum energy path of different dislocations in different systems. In pure crystals, Al, Ni, and Cu, a variation of ZPE with the same magnitude as the Peierls barriers but with opposite sign indicates that dislocations may glide with weaker resistance due to quantum fluctuations in the 3 different crystals. This result generalizes what was found for the specific case of screw dislocation in bcc Fe [7]. We believe that the ubiquity of ZPE in various simulations for different model materials, with always the same trend, can be viewed as a confirmation of the physical realism of such an effect. It is particularly important to multiply the different system because of the uncertainty of interatomic potentials used in the simulations. In solid solutions Al(Mg) or Cu(Ag), the same trend has been observed although the ZPE variation ratio to the potential energy barrier is less important than in pure crystals. In Al(Mg) such a ratio is about one tenth while in Cu(Ag) it falls to one hundredth. The integration of the Orowan equation has allowed us to show that quantum effects yield a softening at low temperature. However we have not identified any inversion of the slope of the stress-temperature curve as was observed experimentally [39,40]. Even though our theoretical assumptions about the statistics of solid solution seem rather rough and would require some consolidations, our results indicate that the ZPE variation is not the main reason for the inversion of the stress-temperature curve observed experimentally in various fcc solid solutions.

Finally, we have tested the Einstein approximation to compute the ZPE in different systems. The satisfactory agreement between the Einstein approximation and the exact ZPE calculation shows that the main quantum contribution comes from vibrational modes with short wavelengths. We interpret such a result as the fact that the interaction between the acoustic modes, i.e., with long wavelengths, and the dislocations can be neglected. Such a result confirms what was found in bcc Fe [7] where the ZPE variation could be computed from a truncated Hessian matrix, restricted to few atoms situated around the dislocation core. However our computation of the quantum effect relying solely on the harmonic approximation calls for a more sophisticated method to properly determine the quantum dislocation glide. To that purpose, some approaches, based on the imaginary time path integrals [41], could be employed latter on, such as the centroid method [42,43] or the reversible work method [44].

ACKNOWLEDGMENT

We gratefully acknowledge Lisa Ventelon for her enlightening remarks.

APPENDIX : TEMPERATURE VARIATION OF CRITICAL SHEAR STRESS IN Al(Mg)

We use the transition state theory to integrate the Orowan equation [7]: $\dot{\epsilon} = \rho_d b \bar{V}$, which relates the deformation rate $\dot{\epsilon}$ to the mobile dislocation density ρ_d and the average velocity of these dislocations $\bar{V}$. As in experimental tests, we have fixed $\dot{\epsilon} = 7 \times 10^{-4}$ s^{-1} [39]. Neglecting the traveling time of dislocations between two successive anchored configurations, we can write the average velocity as $\bar{V} = d\Gamma$ where d is the distance between two successive anchored configurations and Γ is the frequency of dislocation depinning from solute atoms through thermally activated process. To estimate d and Γ we employ a series of rather rough approximations allowing us to work out the profile of the stress-temperature curve only from atomic scale data. However we keep clearly in mind that our theoretical treatment needs to be refined on several aspects. In a solid solution [24], we remark that the dislocations pass the anchoring configurations by crossing

first the weakest obstacle along its line. Then the dislocation segments in close interaction with this obstacle form a bulge which extends all along the dislocation line. We estimate the jump frequency Γ associated with this process by considering an atomic simulation cell with a segment of edge dislocation of a given length $L_{\rm sim}$ in interaction with a single solute atom. We have verified that the final result is not modified taking different values for $L_{\rm sim}$.

According to the classical transition state theory [45], the rate Γ for a three-dimensional system made of $N_{\rm at}$ atoms of equal mass m is expressed as an integral over the system phase space

$$\Gamma = \frac{1}{Z_r}\int \prod_{i=1}^{3N_{\rm at}} \frac{dX_i dP_i}{h^{3N_{\rm at}}} \delta(\mathbf{X}-\mathbf{X_s}) \frac{|\mathbf{P}\cdot\mathbf{d}_s|}{m} \theta(\mathbf{P}\cdot\mathbf{d}_s) \times e^{[-\beta\mathcal{H}(\mathbf{P},\mathbf{X})]}, \quad \text{(A1)}$$

where thick symbols stand for $3N_{\rm at}$-dimensional vectors, $\mathbf{X}$ represents the atomic positions, while $\mathbf{P}$ is the associated momentum. $\mathbf{X}_s$ is the atomic configuration associated with the transition state, i.e., the unstable dislocation configuration between Peierls valleys, $\mathbf{d}_s$ is the corresponding unstable eigenmode, $\mathcal{H}(\mathbf{P},\mathbf{X})$ is the Hamiltonian of the system to which the work of the applied stress is properly subtracted, and Z_r is the reactant partition function, i.e., the harmonic partition function of the crystal with a dislocation at rest. The functions δ and θ are the standard Dirac and Heaviside functions, respectively. Following the same treatment as in [7], we obtain

$$\Gamma = \frac{k_B T}{h} \frac{h\beta\nu_s/2}{\sin(h\beta\nu_s/2)} \frac{\prod_{i=1}^{3N_{\rm at}-3}\left[2\sinh\left(\frac{h\beta}{2}\vartheta_i\right)\right]}{\prod_{j=1}^{3N_{\rm at}-4}\left[2\sinh\left(\frac{h\beta}{2}\nu_j\right)\right]} e^{-\beta H_D}, \quad \text{(A2)}$$

where H_D represents the activation enthalpy for crossing the obstacle, and ϑ_i and ν_j are the eigenfrequencies of the system at rest and at the saddle state, respectively. In comparison with [7], we notice that the Goldstone mode is absent from our problem because there is no translational symmetry in the present case as the dislocation is supposed to pass the pinning configuration by crossing an isolated obstacle along its line. To estimate the activation enthalpy H_D, we develop H_D with respect to the applied stress σ, which yields the standard linear equation

$$H_D = \Delta E - \sigma b A^*, \quad \text{(A3)}$$

where A^* is known as the activation area, and ΔE is the energy barrier estimated from our computations with a single solute atom in interaction with the dislocation. The sole parameters we have to determine for the solid solution are thus A^* and d, the distance between anchored configurations. To that purpose we just remark that H_D must be zero when the applied stress σ reaches the critical shear stress σ_c, such that $A^* = \Delta E/\sigma_c b$. The accurate computation of σ_c is very difficult and it is not analytical [15]. Here we choose for the sake of simplicity to estimate roughly σ_c from the stress required to pass a regular row of obstacles distant from the average distance between solute atoms $d_{\rm sol} = a/c$, where a is the lattice distance along the dislocation line and c is the atomic concentration of impurity. The force equilibrium condition between the Peach and Koehler forces and the obstacle forces, denoted by f_o, yields the equality $\sigma_c = f_o c/(ba)$. Applying the same in the case of our simulation we obtain $\sigma_{\rm sim} = f_o/bL_{\rm sim}$, where $\sigma_{\rm sim}$ stands for the critical shear stress applied to our simulation cell to force the dislocation glide. We therefore approximate the critical stress of the solid solution by $\sigma_c = c\sigma_{\rm sim}L_{\rm sim}/a$. We also estimate the distance between anchored configurations d from the distance between solute atoms $d_{\rm sol}$ through the assumption of proportionality, recognizing that the larger the concentration, the shorter the distance between anchored configurations. In the direction of glide for the edge dislocation we have $d \approx b/c$. After having recognized from the efficiency of the Einstein approximation [Eq. (7)] that the acoustic modes, i.e., of low frequencies and large wavelengths, do not interact with the dislocation and that the frequency associated with the unstable mode of the saddle state verifies $\omega_s \ll k_B T/\hbar$, one can reduce Eq. (A2) to obtain

$$\Gamma = \frac{k_B T}{h} \frac{\prod_{\vartheta_i>\omega_t}\left[2\sinh\left(\frac{h\beta}{2}\vartheta_i\right)\right]}{\prod_{\nu_j>\omega_t}\left[2\sinh\left(\frac{h\beta}{2}\nu_j\right)\right]} e^{-\beta\Delta E(1-\sigma/\sigma_c)}, \quad \text{(A4)}$$

where ω_t corresponds to the frequency threshold above which the vibrational modes are affected by the presence of the dislocation glide. A low-temperature approximation with the thermal energy $k_B T$ small compared to $\hbar\omega_t/2$ leads to $2\sinh(\frac{h\beta}{2}\vartheta_i) \approx \exp(\frac{h\beta}{2}\vartheta_i)$, whereas within classical approximation $k_B T \gg h\vartheta_i/2$ leads to $2\sinh(\frac{h\beta}{2}\vartheta_i) \approx h\vartheta_i\beta$. At low temperature we thus obtain the formula

$$\Gamma = \frac{k_B T}{h} e^{-\beta[\Delta E(1-\sigma/\sigma_c)+\delta Z_s]}, \quad \text{(A5)}$$

where δZ_s stands for the ZPE difference between the saddle state and the ground state. The Orowan equation can be rewritten with help of Eq. (A5):

$$\dot\epsilon = \rho_d \frac{b^2}{c} \frac{k_B T}{h} e^{-\beta\{\Delta E[1-a\sigma/(c\sigma_{\rm sim}L_{\rm sim})]+\delta Z_s\}}, \quad \text{(A6)}$$

and after using the rough approximations for $\sigma_c = c\sigma_{\rm sim}L_{\rm sim}/a$ and $d = b/c$, it can be solved analytically:

$$\sigma = \frac{\sigma_{\rm sim} c L_{\rm sim}}{a\Delta E}\left[\Delta E + \delta Z_s + k_B T \ln\left(\dot\epsilon \frac{ch}{\rho_d b^2 k_B T}\right)\right]. \quad \text{(A7)}$$

At high temperature we proceed similarly but with the classical approximation we obtain from Eq. (A4) the following expression for the crossing rate:

$$\Gamma = \nu_0 e^{-\beta[\Delta E(1-\sigma/\sigma_c)]}, \quad \text{(A8)}$$

where $\nu_0 = \frac{\prod_{i=1}^{3N_{\rm at}-3}[\vartheta_i]}{\prod_{j=1}^{3N_{\rm at}-4}[\nu_j]}$ is usually of the order of the Debye frequency. The Orowan equation can be rewritten with the help of Eq. (A8):

$$\dot\epsilon = \rho_d b d \nu_0 e^{-\beta\Delta E(1-a\sigma/\sigma_c)}, \quad \text{(A9)}$$

which leads to the analytical expression for the applied stress:

$$\sigma = \frac{\sigma_{\rm sim} c L_{\rm sim}}{a\Delta E}\left[\Delta E + k_B T \ln\left(\dot\epsilon \frac{c}{\rho_d b^2 \nu_0}\right)\right]. \quad \text{(A10)}$$

From the comparison between Eq. (A7) and Eq. (A10) one remarks that a negative ZPE variation $\delta Z_s < 0$ such as the one found for the edge dislocation in Al(Mg) implies a reduction of σ in comparison to classical approximation. Indeed the difference between the quantum theory Eq. (A7) and the classical

estimations Eq. (A10) is given by $[\delta Z_s + k_B T \ln(\nu_0 h/k_B T)]$ which tends to equal $[\delta Z_s]$ for sufficiently low temperatures.

Using our simulation data for the Al(Mg) system in order to estimate the parameters of Eq. (A7) and Eq. (A10), we have determined the critical shear stress for different concentrations at different temperatures. Our results are reported in Fig. 5. In comparison to the classical calculation we found that the quantum fluctuations yield a reduction of the critical shear stress for dislocations crossing obstacles. However, we have found no inversion of the stress-temperature curve at low temperature like that evidenced experimentally [39]. Our comparison of the predictions made from Eq. (A7) with experimental data from [39] and [40] shows that we obtain the correct magnitude for the critical stress but the uncertainty is still too large to validate our theoretical approach.

[1] G. Schöck, in *Dislocations in Solids*, Vol. 3, edited by F. R. N. Nabarro (North-Holland, Amsterdam, 1980), pp. 63–163.
[2] T. Suzuki, J. Phys. Soc. Jpn. **64**, 2817 (1995).
[3] Z. S. Basinski, Proc. R. Soc. London, Ser. A **240**, 229 (1957).
[4] E. Bitzek and P. Gumbsch, Mater. Sci. Eng. A **400-401**, 40 (2005).
[5] T. D. Swinburne, S. L. Dudarev, S. P. Fitzgerald, M. R. Gilbert, and A. P. Sutton, Phys. Rev. B **87**, 064108 (2013).
[6] D. Rodney, Phys. Rev. B **76**, 144108 (2007).
[7] L. Proville, D. Rodney, and M. Marinica, Nat. Mater. **11**, 845 (2012).
[8] B. Barvinschi, L. Proville, and D. Rodney, Modell. Simul. Mater. Sci. Eng. **22**, 025006 (2014).
[9] M. I. Baskes, Phys. Rev. B **46**, 2727 (1992).
[10] F. Ercolessi and J. Adams, Europhys. Lett. **26**, 583 (1994).
[11] A. Haziot, X. Rojas, A. D. Fefferman, J. R. Beamish, and S. Balibar, Phys. Rev. Lett. **110**, 035301 (2013).
[12] D. Caillard, Acta Mater. **62**, 267 (2014).
[13] L. Ventelon and F. Willaime, Philos. Mag. **90**, 1063 (2010).
[14] W. Curtin, D. Olmsted, and L. Hector, Nat. Mater. **5**, 875 (2006).
[15] L. Proville and S. Patinet, Phys. Rev. B **82**, 054115 (2010).
[16] L. Ventelon, F. Willaime, E. Clouet, and D. Rodney, Acta Mater. **61**, 3973 (2013).
[17] Y. Mishin, M. J. Mehl, D. A. Papaconstantopoulos, A. F. Voter, and J. D. Kress, Phys. Rev. B **63**, 224106 (2001).
[18] G. P. Purja Pun and Y. Mishin, Philos. Mag. **89**, 3245 (2009).
[19] X.-Y. Liu, P. P. Ohotnicky, J. B. Adams, C. L. Rohrer, and J. R. W. Hyland, Surf. Sci. **373**, 357 (1997).
[20] X.-Y. Liu, J. B. Adams, F. Ercolessi, and J. Moriarty, Modell. Simul. Mater. Sci. Eng. **4**, 293 (1996).
[21] P. L. Williams, Y. Mishin, and J. C. Hamilton, Modell. Simul. Mater. Sci. Eng. **14**, 817 (2006).
[22] D. J. Bacon, Y. N. Osetsky, and D. Rodney, in *Dislocations in Solids*, edited by J. Hirth and L. Kubin (Elsevier, Amsterdam, 2008).
[23] D. Rodney and G. Martin, Phys. Rev. B **61**, 8714 (2000).
[24] S. Patinet and L. Proville, Phys. Rev. B **78**, 104109 (2008).
[25] D. Rodney and L. Proville, Phys. Rev. B **79**, 094108 (2009).
[26] J. Hirth and J. Lothe, *Theory of Dislocations* (Wiley Interscience, New York, 1982).
[27] D. Rodney, Nucl. Instrum. Methods Phys. Res., Sect. B **228**, 100 (2005).
[28] W. C. Swope, H. C. Andersen, P. H. Berens, and K. R. Wilson, J. Chem. Phys. **76**, 637 (1982).
[29] M. Finnis, MRS Bull. **37**, 477 (2012).
[30] P. A. Gordon, T. Neeraj, and M. I. Mendelev, Philos. Mag. Lett. **91**, 3931 (2011).
[31] C. Woodward, D. R. Trinkle, L. G. Hector, and D. L. Olmsted, Phys. Rev. Lett. **100**, 045507 (2008).
[32] L. Romaner, C. A.-Draxl, and R. Pippan, Phys. Rev. Lett. **104**, 195503 (2010).
[33] G. Henkelman, G. Jóhannesson, and H. Jónsson, *Progress in Theoretical Chemistry and Physics* (Kluwer Academic Publishers, Dordrecht, 2000), p. 269.
[34] R. Gröger and V. Vitek, Mater. Sci. Eng. A **643**, 203 (2015).
[35] L. Dezerald, D. Rodney, E. Clouet, L. Ventelon, and F. Willaime, Nat. Commun. **7**, 11695 (2016).
[36] E. Anderson, Z. Bai, C. Bischof, S. Blackford, J. Demmel, J. Dongarra, J. Du Croz, A. Greenbaum, S. Hammarling, A. McKenney, and D. Sorensen, *LAPACK Users' Guide*, 3rd ed. (Society for Industrial and Applied Mathematics, Philadelphia, PA, 1999).
[37] S. Patinet and L. Proville, Philos. Mag. **91**, 1581 (2011).
[38] H. Chamati, N. Papanicolaou, Y. Mishin, and D. Papaconstantopoulos, Surf. Sci. **600**, 1793 (2006).
[39] V. P. Podkuyko and V. V. Pustovalov, Cryogenics **18**, 589 (1978).
[40] Z. Basinski, R. Foxall, and R. Pascual, Scr. Metall. **6**, 807 (1972).
[41] R. P. Feynman and A. R. Hibbs, *Quantum Mechanics and Path Integrals* (McGraw-Hill, New York, 1965).
[42] M. J. Gillan, Phys. Rev. Lett. **58**, 563 (1987).
[43] M. J. Gillan, Philos. Mag. A **58**, 257 (1988).
[44] G. Mills, H. Jónsson, and G. K. Schenter, Surf. Sci. **324**, 305 (1995).
[45] W. Miller, J. Chem. Phys. **62**, 1899 (1975).